Synthesis routes for enhanced piezoelectric properties in spark plasma sintered Ta-doped KNN ceramics

Marion Dubernet, Michael J Pitcher, Mustapha Zaghrioui, Micka Bah, Julien Bustillo, Fabien Giovannelli, Isabelle Monot-Laffez

Synthesis routes for enhanced piezoelectric properties in spark plasma sintered Ta-doped KNN ceramics

Marion Dubernet[a,*], Michael J. Pitcher[b], Mustapha Zaghrioui[a], Micka Bah[a], Julien Bustillo[a], Fabien Giovannelli[a], Isabelle Monot-Laffez[a]

[a] *GREMAN UMR 7347, Université de Tours - CNRS - INSA-CVL, Tours, 37200, France*
[b] *CEMHTI UPR 3079, CNRS - Université d'Orléans, Orléans, 45071, France*

Abstract

Ta Substitution in $K_{0.5}Na_{0.5}NbO_3$ lead free piezoelectrics helps to prevent grain growth and has been shown to improve the piezoelectric properties. Two synthesis routes have been studied to prepare $K_{0.5}Na_{0.5}Nb_{0.8}Ta_{0.2}O_3$ (KNNTa) substituted powders. Then highly densified KNNTa ceramics have been obtained by Spark Plasma Sintering (SPS). The use of a synthesized oxide precursor $Nb_{1.6}Ta_{0.4}O_5$ during the ceramic elaboration process clearly shows through accurate Rietveld study a successful Ta substitution with 92% of *Amm2* $K_{0.485(8)}Na_{0.515(8)}Nb_{0.819(6)}Ta_{0.181(6)}O_3$ phase, confirmed by SEM-EDS analysis and a more homogeneous chemical composition. This leads to enhanced electromechanical coupling coefficients with an improvement of 50% of k_t, 15% for k_p and low electrical losses, compared to the conventional method with a simple mixing of commercial precursors.

Keywords: Lead-free ceramics, Spark Plasma Sintering, Piezoelectric properties, KNN

1. Introduction

Piezoelectricity is a physical phenomenon which converts a mechanical action into electricity and vice versa. Piezoelectric materials are used to fabricate sensors or actuators and can be from natural origin such as quartz or synthetic origin such as the lead titanate and zirconate (PZT) which has dominated the piezoelectric market up to now. Due to its toxicity, the use of lead is regulated by the REACH restrictions. Perovskite materials such as (Bi,Na)TiO_3 (BNT), (K,Na)NbO_3 (KNN), (Ba,Ca)(Ti,Zr)O_3 (BCTZ) are well-known to exhibit piezoelectric properties and have been studied extensively as promising candidates to replace PZT materials [1–4]. These past years, research interest in KNN system compo-

*Corresponding author
Email address: marion.dubernet@univ-tours.fr (Marion Dubernet)

sitions has increased because of their ferroelectric properties, their high Curie temperature ($\approx$ 400 °C) and their attractive electromechanical coupling coefficients. This system exhibits tetragonal, orthorhombic and rhombohedral ferroelectric phases and a morphotropic phase boundary (MPB) between two orthorhombic phases around the $K_{0.5}Na_{0.5}NbO_3$ composition [1]. However, the dielectric and piezoelectric properties are highly dependent on the densification composition of the materials. KNN ceramics are difficult to densify due to the volatilization of potassium and sodium elements leading to a change in composition at high temperatures and long holding times (up to 10 h) encountered with conventional sintering methods. It was shown that Na/K ratio plays a key-role in the KNN ceramic consolidation which leads to a competition between densification and grain growth phenomenon [5–9]. However, high densities of KNN-based systems were obtained using an alternative Spark Plasma Sintering (SPS) technique [10–14]. This process combines a high pressure and a rapid heating rate to decrease the sintering temperature and time. Moreover, addition or/and substitution with Zr, Cu, Co, Mn, Li, Sr, Ta etc... have been investigated to enhance densification [10, 15–23]. Among them, tantalum substitution at 10 to 20% has been shown to effectively reduce grain growth and to gradually decrease the ortho-tetragonal transition and the Curie temperatures, leading to slightly increased piezoelectric properties [24–28]. However, for these Ta substitutions, difficulties were uncounted to densify ceramics and alternative processes were investigated (reactive template grain growth method, microwave hydrothermal technique) [24, 27]. Jean *et al.* have shown that, for 20 to 30 % Ta substitution on Nb-site combined with SPS technique, the piezoelectric properties have been sensitively improved compared to undoped KNN compositions. Moreover, the structure is shown to evolve from an orthorhombic to a tetragonal phase but for a Ta substitutions as low as 5%, the cationic composition appears heterogeneous with difficulties to homogeneously incorporate Ta to KNN structure [10].

In the present work, two routes were followed in order to improve the chemical composition using on the one hand the conventional precursors Nb_2O_5/Ta_2O_5 and on the other hand, a $Nb_{1.6}Ta_{0.4}O_5$ precursor as suggested by Wang *et al.* [15]. Severeal papers dealing with K-Na-Nb-Ta-O compositions do not show any microstructures. Some others report that even

after 24 h attrition milling and calcination repeated two times, the conventional synthesis and sintering route exhibit heterogeneous composition. To limit the volatility of the alkali metals Na and K, the SPS process was used because it allows to decrease the densification temperature and time while it fully consolidates the ceramics. The piezoelectric properties of the two different Ta-doped KNN ceramics as well as unsubstituted KNN prepared with the same process were then measured and compared.

2. Material and methods

Two batches of the composition $K_{0.5}Na_{0.5}Nb_{0.8}Ta_{0.2}O_3$ were synthesized by conventional solid state reaction. The first batch (referred to as "KNNTa") was prepared by mixing the starting materials K_2CO_3 (99+%, ChemPUR), Na_2CO_3 (99.9+%, ChemPUR), Nb_2O_5 (99.9%, ChemPUR) and Ta_2O_5 (99.9%, ChemPUR) in an agate planetary ball mill for 15 min at 300 rpm. The powder mixture was then calcined twice at 830 °C for 5 h under air with intermediate grinding. After both calcinations, the powders were reground with the same procedure. For the second batch (referred to as "KNNTa-prec"), a special precursor $Nb_{1.6}Ta_{0.4}O_5$ was first prepared: niobium and tantalum oxides were mixed by ball-milling for 15 min at 300 rpm and calcined twice at 1200 °C for 6 h, determined by DTA control and then finally reground. This precursor was then mixed with potassium and sodium carbonates in appropriate proportions to obtain the same final composition. Subsequent calcination and grinding steps were then identical to the first batch (KNNTa) preparation. The grain size distribution of both batches was measured by laser granulometer (HORIBA) using Fraunhaufer mathematical method.

Densification experiments were performed with a Spark Plasma Sintering equipment (DR. SINTER LAB 632-LX, SPS Fuji Electronics, Japan). The calcined powders were introduced into a 15 mm diameter graphite die. Carbon foil was used at the interfaces between the powder, the graphite die and both punches to maintain a good electrical contact between the powder and the graphite materials and to facilitate the removal of the sample after the sintering. An uniaxial pressure of 50 MPa was first applied in one minute under argon atmosphere. The temperature was then increased from room temperature up to 960 °C (previously optimized [10]) with a heating rate of 100 °C/min, followed by an isothermal

dwell of 3 to 5 min suffisant to get complete densifications and the insitu displacement curve was registred. In a third step, the pressure was decreased to 0.3 MPa and the temperature to 20 °C in 9 min. After sintering, the pellets were polished to 1 mm in thickness with plane-parallel faces. Due to reducing conditions during SPS runs, the samples exhibit conduction properties because of an oxygen deficiency. A thermal treatment was carried out up to 900 °C with 2 h dwell under oxygen flow in order to remove carbon contamination from the die and to fully oxygenate the samples [29].

Microstructures of powders and sintered samples were observed by scanning electron microscopy (TESCAN-MIRA 3 SEM) with secondary electrons (SE) and back-scattered electrons (BSE) detectors and the compositions were measured by energy-dispersive X-ray spectroscopy analysis (EDS Oxford Instrument AZTec). The density of the sintered ceramics was measured by the Archimedes method using a MS204TS/00 analytical balance (METTLER TOLEDO) in distilled water.

Laboratory powder X-ray diffraction (PXRD) for phase analysis was carried out on a Bruker D8 Advance diffractometer in Bragg-Brentano geometry, using CuKα_1/Kα_2 radiation, with powders dispersed on a Si wafer. Rietveld refinements were carried out on synchrotron X-ray diffraction data (SPD) collected at ambient temperature at beamline 11BM (APS, Argonne, U.S.A.). An incident wavelength $\lambda = 0.45806$ Å was used. To minimise absorption effects, the samples were loaded in borosilicate capillaries of diameter 0.3 mm, which in turn were contained within Kapton capillaries of 0.8 mm diameter. The capillaries were spun during the measurement. Rietveld analysis was carried out using TOPAS Academic (v.6). Additionally, these samples were analysed by energy-dispersive spectroscopy (EDS) using a Philips CM20 transmission electron microscope fitted out with an Oxford EDS analyser.

In order to measure piezoelectric properties of the sintered samples, silver paint was deposited on both sides of the polished pellet and annealed at 700 °C for 2 h for adhesion by slight diffusion of the electrodes into the ceramic surface. The ceramics were then poled at 120 °C and the voltage was increased up to 3 kV/mm with a ramp of 120 V/min and field cooled for about 45 min. The Bode analysis of impedance measurements using KLM model allows to extract all the following piezoelectric constants [30, 31]: the velocity v, the

planar coupling coefficient k_p, the thickness coupling coefficient k_t, the dielectric constant ε, the electrical losses δ_{el} and the mechanical quality factor Q_m.

In addition, the same analyses have been conducted on undoped KNN ceramics previoulsy studied and prepared in similar conditions, for comparison [10, 32].

3. Results and discussion

3.1. Microstructural considerations

Fig. 1 shows the SEM images of KNNTa and KNNTa-prec powders prior to Spark Plasma Sintering. The grain morphology of the powders show the presence of submicron grains and some coarse particles on the SE images (Fig. 1a and 1c). The grain size appears slighty larger for the KNNTa-prec and this result is confirmed by laser granulometry measurement where the mean diameter was found, respectively, at 0.52 µm and at 0.71 µm for KNNTa and KNNTa-prec powders. This is due to the use of the refractory $Nb_{1.6}Ta_{0.4}O_5$ precursor in the synthesis method. Moreover, the grain size distributions for both of KNNTa samples are monomodal with the same grain size range (0.37 to 1.9 µm).

However on Fig. 1b, BSE images show the presence of smaller white grains revealing a different composition. EDS analysis reveals that these grains are composed of K, Na, Nb, Ta but largely enriched in tantalum element compared to the nominal stoichiometry with average composition ($K_{0.40}Na_{0.60}Nb_{0.29}Ta_{0.70}O_3$). On the contrary, these tantalum-rich-grains are rarely present when the powder is prepared with $Nb_{1.6}Ta_{0.4}O_5$ precursor (Fig. 1d). This first result shows that the tantalum incorporation into the KNN structure is improved by the use of KNNTa-prec preparation.

Consolidations of KNNTa and KNNTa-prec powders were carried out by SPS and the shrinkage curves during the sintering were plotted versus temperature (Fig. 2). The calculated relative density is over 96% for all samples. The sintering of KNNTa and KNNTa-prec starts respectively at 630 °C and at 780 °C indicating that the consolidation temperature is higher for KNNTa-prec. This can be linked to the grain size which is slightly larger in the case of KNNTa-prec powder or the refractory aspect of the $Nb_{1.6}Ta_{0.4}O_5$ precursor synthesized at 1200 °C. Then, for this latter, considering the shrinkage slopes, the densification speed is faster and it can be related to the more homogeneous composition of this powder,

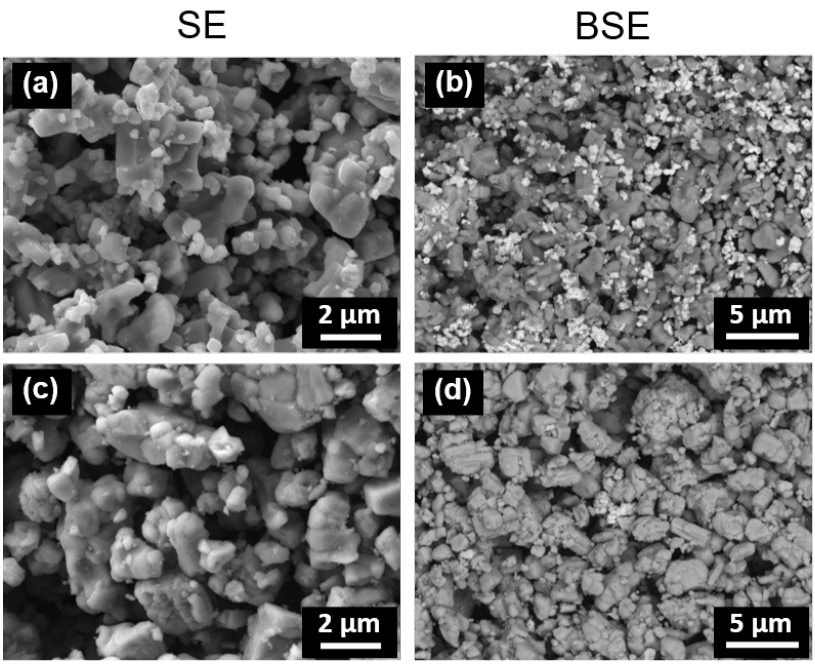

Figure 1: SEM images of $K_{0.5}Na_{0.5}Nb_{0.8}Ta_{0.2}$ powders for : (a), (b) KNNTa and (c), (d) KNNTa-prec. The images (a), (c) and (b), (d) were respectively recorded in secondary electron mode (SE) and in back scattering electron mode (BSE).

modifying the diffusion process. However, the shrinkage segment is similar for both samples leading to a comparable relative density.

Fracture and polished surfaces of the sintered ceramics KNNTa and KNNTa-prec were then observed from BSE mode (Fig. 3). The atomic number contrast suggests three crystalline phases for KNNTa samples (Fig. 3a) which can be identified : white, black and grey. On the other hand, KNNTa-prec tends to be more homogeneous although smaller white areas are visible. The use of $Nb_{1.6}Ta_{0.4}O_5$ precursor clearly improves the composition homogeneity and reduces the number and the size of the white areas observed on the KNNTa ceramics (Fig. 3a and 3b). Cross section images confirm the slightly larger grain size in the KNNTa-prec sample and the same phase distribution than the sample surfaces. The role of Ta as grain growth inhibitor is clearly illustrated here.

To complete the SEM characterization, EDS analysis were conducted on the polished surface samples to determine the cationic atomic composition of each different region shown in Fig. 3. The atomic variations of the KNNTa and KNNTa-prec ceramics in potassium,

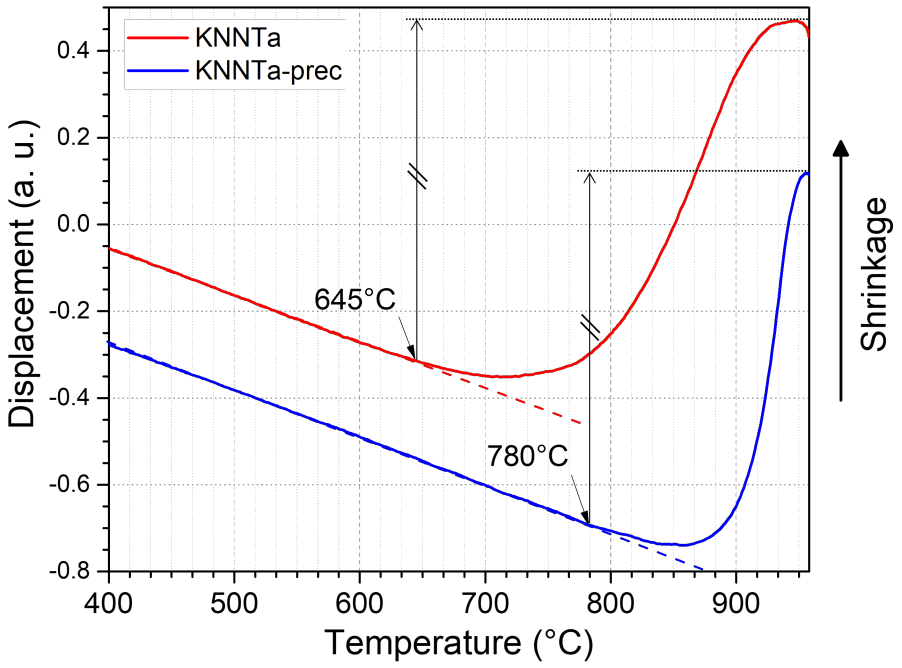

Figure 2: Shrinkage curves of the KNNTa and KNNTa-prec powder densification during SPS process. Origins of the curve are different for visibility. Y axis represents the punch displacement and the black arrows the total shrinkage of both samples.

sodium, niobium and tantalum elements along a line are represented on Fig. 4. A point was recorded every 10 µm.

For KNNTa samples (Fig. 4a), the white and the dark inclusions correspond respectively to a Ta-rich ($K_{0.4}Na_{0.6}Nb_{0.3}Ta_{0.7}O_3$) and a Nb-rich ($K_{0.5}Na_{0.5}Nb_{0.99}Ta_{0.01}O_3$) composition with K and Na content close to the stoichiometric ratio. On the micrograph, the grey region with the composition $K_{0.53}Na_{0.47}Nb_{0.85}Ta_{0.15}O_3$ seems to be a mixture between the white and the dark phases. Indeed, small fluctuations of Ta and Nb are clearly visible in this region but it could be due to the pear-shaped area volume where the electron matter interactions occur below the sample surface. In comparison, the element variations for KNNTa-prec ceramics are smoother (Fig. 4b) which is in agreement with the BSE image in Fig. 3b. The grey region has a composition close to the nominal one and the white inclusions correspond to a Ta-rich phase ($K_{0.67}Na_{0.33}Nb_{0.60}Ta_{0.40}O_3$), which is different to the composition observed on the KNNTa ceramics. On the contrary, the dark Nb-rich phase is not present in KNNTa-prec. As conclusion, the cationic composition was clearly improved and homogenized by the

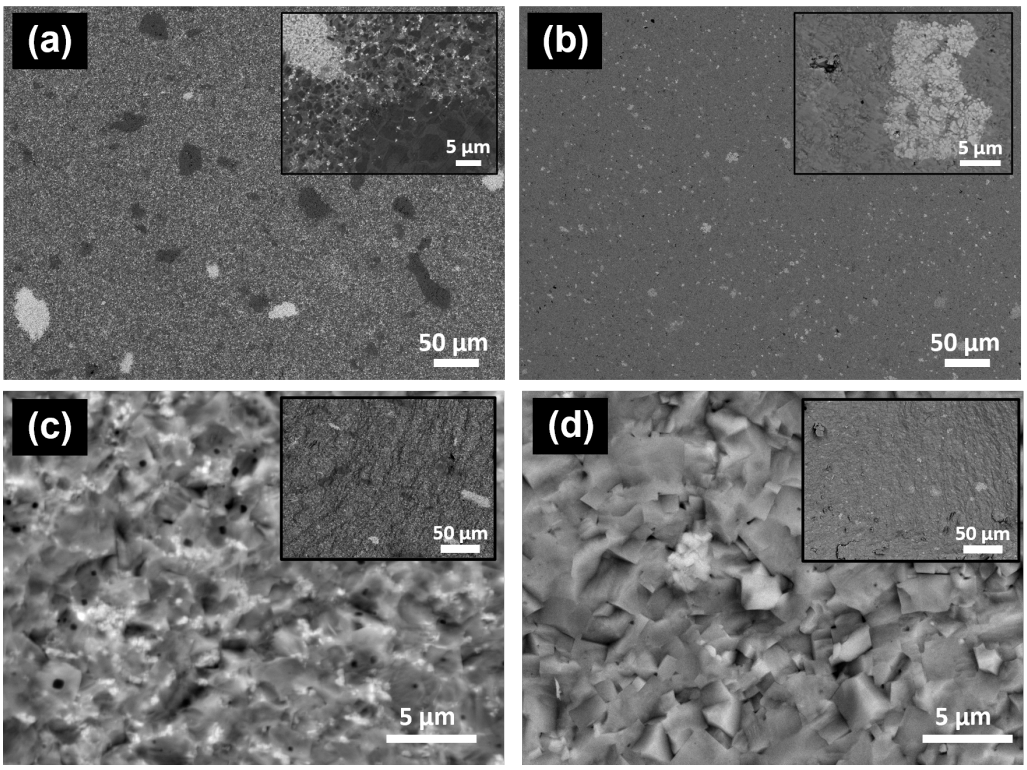

Figure 3: SEM-BSE images of the surface of (a) KNNTa and (b) KNNTa-prec and the cross sections of (c) KNNTa and (d) KNNTa-prec microstructures. The insert images show the surface of the ceramics at higher magnitude and near the white areas.

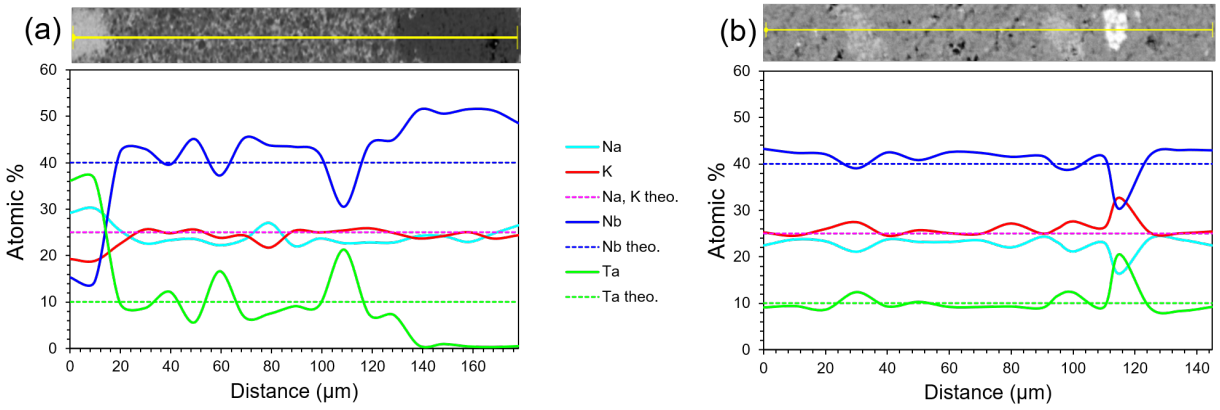

Figure 4: EDS elemental line-scan profiles of Na, K, Nb and Ta : (a) KNNTa and (b) KNNTa-prec. The dot lines correspond to the atomic theoretical percentages calculated from the nominal $K_{0.5}Na_{0.5}Nb_{0.8}Ta_{0.2}$ composition.

use of the $Nb_{1.6}Ta_{0.4}O_5$ precursor.

3.2. X-Ray diffraction

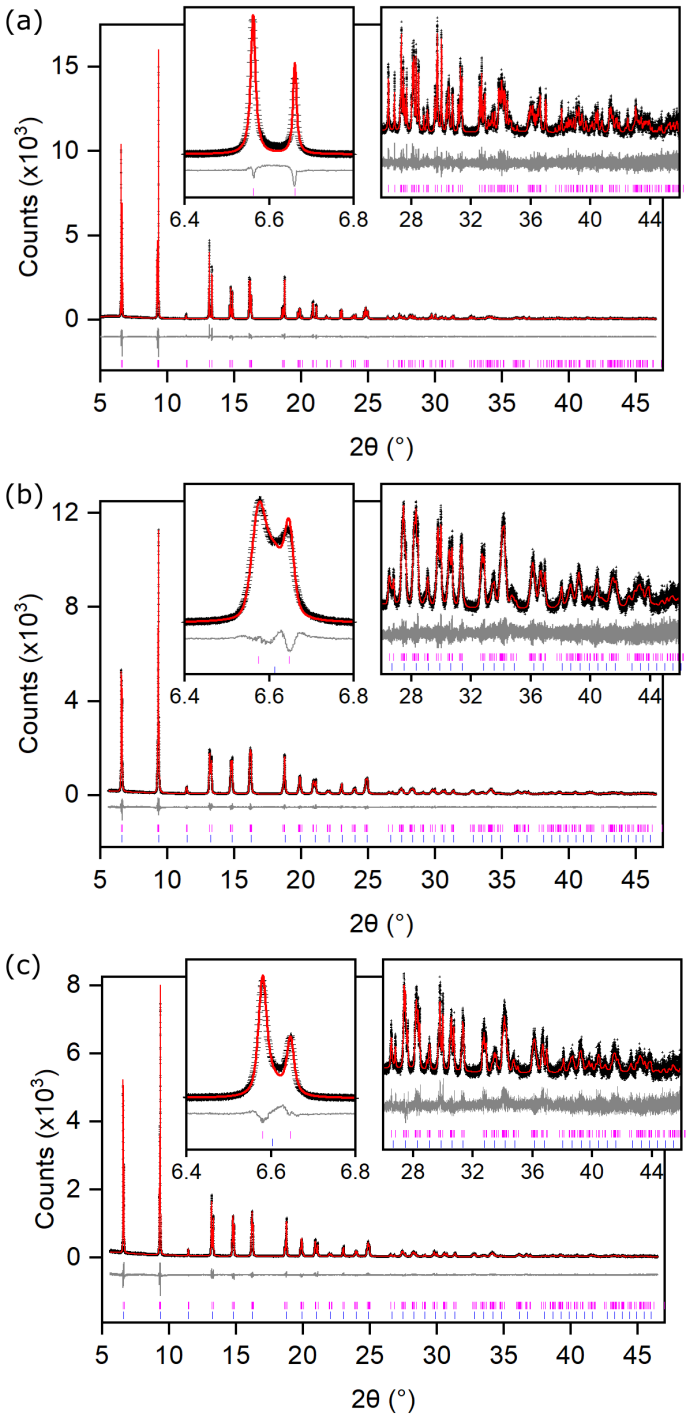

Figure 5: Rietveld refinements against SPD data for (a) KNN fitted to a single *Amm2* perovskite, (b, c) KNNTa and KNNTa-prec fitted to a two-phase mixture of *Amm2* and $Pm\bar{3}m$ perovskites. Magnified views of the (011)/(100) peaks and high-angle regions are shown as insets.

High resolution synchrotron X-ray powder diffraction (SPD) data were collected from reground ceramic fragments of KNNTa and KNNTa-prec pellets at ambient temperature and analysed by Rietveld refinement. For comparison, an un-doped KNN sample ($K_{0.5}Na_{0.5}NbO_3$) was confirmed to be a single-phase material, with a good fit provided by the literature *Amm2* perovskite structure (Fig. 5a).

For KNNTa, attempts to refine a single *Amm2* perovskite phase produced an unsatisfactory Rietveld fit (Fig. S1a). In particular, at low angles this model failed to fit the observed intensity between (011) and (100) peaks of the *Amm2* cell, whose splitting is characteristic of the orthorhombic distortion (a_p x $\sqrt{2}a_p$ x $\sqrt{2}a_p$) of the primitive cubic perovskite cell a_p in KNN (Fig. S1a, inset). This implies the presence of an additional perovskite phase of cubic (or near-cubic) symmetry and might correspond to MPB phases as refered in the KNN phase diagram. A second perovskite phase (referred to as "Phase 2") was therefore included in the refinement, and assigned to a simple cubic perovskite structure ($Pm\overline{3}m$, fixed atomic coordinates) as shown in our previous study [10]. The initial compositions of Phase 1 and Phase 2 were both set to the nominal composition of the sample ($K_{0.5}Na_{0.5}Nb_{0.8}Ta_{0.2}O_3$) and their initial scale factors were weighted equally, with a global compositional constraint allowing the cation sites to be refined whilst retaining an overall composition of $K_{0.5}Na_{0.5}Nb_{0.8}Ta_{0.2}O_3$. Three isotropic atomic displacement parameters (U_{iso}) were refined for each phase, corresponding to the A-site (Na/K), B-site (Nb/Ta) and O sites, with soft constraints to ensure comparable and physically reasonable values for both phases (for example, this assures similar U_{iso} values for the Na/K sites in both phases). This constrained refinement produced a good fit to the data (see Fig. 5b, $\chi^2 = 1.22$), with refined compositions and phase fractions of $K_{0.55(2)}Na_{0.45(2)}Nb_{0.936(8)}Ta_{0.064(8)}O_3$ (74.1(5) mol%) and $K_{0.36(3)}Na_{0.64(3)}Nb_{0.23(2)}Ta_{0.77(2)}O_3$ (25.9(5) mol%) for Phase 1 and Phase 2 respectively (see Table 1).

This indicates that the majority of the Ta dopant is accommodated in a secondary perovskite phase (Phase 2), whilst the majority of the sample corresponds to a KNN-like Nb-rich orthorhombic phase (Phase 1). Direct comparison with the SEM-EDS analysis previously described in Fig. 4 allows the bright regions of the SEM images to be identified as the Ta-rich cubic perovskite $K_{0.36}Na_{0.64}Nb_{0.23}Ta_{0.77}O_3$ (Phase 2). The interpretation of the dark/grey regions in the SEM images is more subtle: the refined composition of Phase 1 lies half way be-

Site	**x**	**y**	**z**	**Occupancy**	**B_{iso} (Å^2)**	**Mol. %**
Phase 1:						74.1(5)
Na / K	0	0	0	0.45(2) / 0.55(2)	0.79(4)^a	
Nb / Ta	0.5	0	0.504(1)	0.936(8) / 0.064(8)	0.28(1)^b	
O1	0	0	0.480(2)	1	0.68(7)^c	
O2	0.5	0.758(1)	0.222(2)	1	0.68(7)^c	
S.G.: *Amm2*; LPs: a = 3.95036(2), b = 5.63569(5), c = 5.66209(6) Å ; V = 126.055(2) Å^3						
Phase 2:						25.9(5)
Na / K	0	0	0	0.64(3) / 0.36(3)	0.83(8)^a	
Nb / Ta	0.5	0.5	0.5	0.23(2) / 0.77(2)	0.37(1)^b	
O1	0	0.5	0.5	1	0.7(1)^c	
S.G.: $Pm\bar{3}m$; LPs: a = b = c = 3.97114(4) Å; V = 62.625(2) Å^3						

^{a,b,c} Parameters subject to soft constraints

Table 1: Refined structures of the *Amm2* and $Pm\bar{3}m$ phases in KNNTa (R_{wp} = 8.30, χ^2 = 1.22).

tween the compositions obtained by EDS (respectively $K_{0.5}Na_{0.5}Nb_{0.99}Ta_{0.01}O_3$ (dark) and $K_{0.53}Na_{0.47}Nb_{0.85}Ta_{0.15}O_3$ (grey)), which are present in approximately equal proportions. This suggests that Phase 1 (the *Amm2* perovskite) should not be interpreted as an individual discrete phase in the material. Instead, it represents the average of these two regions which both adopt an orthorhombic perovskite structure similar to that of KNN. Indeed, this is confirmed by TEM-EDS data on 21 particles of KNNTa, which shows a wide distribution in the Nb/Ta ratio (Fig. S2), rather than two discrete populations. The presence of multiple phases closed to phase 1 was already observed in KNN-system and can suggest that Ta substitution emphasizes the morphotropic phase boundary phenomenon which is correlated to piezoelectric properties enhancement [33].

The same refinement protocol was then applied to KNNTa-prec, after attempts to fit this high-resolution data to a single-phase model produced similar unsatisfactory Rietveld fits (Fig. S1b). In this case, the fraction of Phase 2 was found to be significantly smaller than that present in KNNTa, and it was thus necessary to fix the composition of this phase to the EDS-derived value of $K_{0.67}Na_{0.33}Nb_{0.59}Ta_{0.41}O_3$ (corresponding to the light regions from SEM scans in Fig. 3). This produced a good fit to the data (see Figure 5c, R_{wp} = 10.21, χ^2 = 1.14). In contrast to KNNTa, the Ta substituant in KNNTa-prec is accommodated primarily

in the majority *Amm2* perovskite phase (Phase 1, 91.9(3) mol.%), whose refined composition of $K_{0.485(8)}Na_{0.515(8)}Nb_{0.819(6)}Ta_{0.181(6)}O_3$ indicates that the phase has been doped successfully with Ta (Table 2). The higher amount of Ta substitution in Phase 1 of KNNTa-prec is also consistent with its refined unit cell volume (125.865(1) Å^3), which is smaller than that of KNN (126.283(1) Å^3, see Table S1) and KNNTa (126.055(2) Å^3) [10, 33]. It can be noticed that the ratio Na/K in this case is reversed compare to phase 1 of the KNNTa sample and it is understood the MPB is intrisquely control by Na/K ratio and that some piezoelectric properties are improved for this ratio superior to 1 [34]. The comparison with SEM-EDS analysis allows us to confirm the majority (grey) regions as *Amm2*, which in this case can be interpreted as a discrete phase (for comparison, see the narrow distribution of Nb/Ta ratio by TEM-EDS on 20 particles on Fig. S2). The relatively low mole fraction of cubic perovskite phase (Phase 2, 8.1 mol.%) is consistent with the lower population of bright areas in the SEM-BSE images, compared with the KNNTa sample and the more homogeneous composition.

Site	**x**	**y**	**z**	**Occupancy**	**B_{iso} (Å^2)**	**Mol. %**
Phase 1:						91.9(2)
Na / K	0	0	0	0.515(8) / 0.485(8)	1.91(4)^a	
Nb / Ta	0.5	0	0.501(2)	0.819(6) / 0.181(6)	0.49(1)^b	
O1	0	0	0.470(3)	1	1.20(7)^c	
O2	0.5	0.758(1)	0.225(3)	1	1.20(7)^c	
S.G.:*Amm2*; LPs: a = 3.95125(2), b = 5.63203(3), c = 5.65595(3) Å ; V = 125.865(1) Å^3						
Phase 2:						8.1(2)
Na / K	0	0	0	0.33 / 0.67 †	1.9(3)^a	
Nb / Ta	0.5	0.5	0.5	0.59 / 0.41 †	0.50(7)^b	
O1	0	0.5	0.5	1	1.2(4)^c	
S.G.: $Pm\bar{3}m$; LPs: a = b = c = 3.9769(1) Å ; V = 62.898(6) Å^3						

^{a,b,c} Parameters subject to soft constraints

†Parameters fixed to EDS-derived values due to small mole fraction of the phase

Table 2: Refined structures of the *Amm2* and $Pm\bar{3}m$ phases in KNNTa-prec (R_{wp} = 10.24, χ^2 = 1.14)

3.3. *Piezoelectric properties*

To determine how the microstructure, through two synthesis methods, can control the piezoelectric properties, several piezoelectric parameters were extracted from impedance measurements and their values are presented in Table 3 for representative samples of each batch. All samples have a high relative density over 97% which is sufficient for reliable and reproductible electrical properties. The velocity v reaches more than 6000 m/s for KNNTa and is increased up to 7000 m/s for KNNTa-prec. No clear conclusion appears in the dielectric constant ε with the two batches; however it can be underlined that these values (between 500 and 600) are more than double those of undoped KNN. The main feature arises for the electromechanical coupling coefficients; k_t is improved by 50% between KNNTa and KNNTa-prec while k_p reached very high values [59 - 50%], corresponding to 15 to 20% more for KNNTa-prec, coupled with red 50% reduced electric losses, as low as 3% [32]. One can conclude that the successful incorporation of Ta (around 20 at.%) and the composition homogeneity improvement are effective to improve the coupling coefficients in KNNTa in both directions and reduce the electrical losses. For what concerns the mechanical losses, no clear trends appear and the quality factor linked to these losses is about 45-50%. Thus, KNNTa-prec ceramics are more suitable for low power applications such as transducers for medical imaging than for high power applications such as sensors which require high Q_m values.

Sample	**Relative density** (%)	**v (m/s)**	ε	$\mathbf{k}_t$ (%)	$\mathbf{k}_p$ (%)	**Electric loss** (%)	$\mathbf{Q}_m$
KNN [11, 32]	97	6534	319	29	48	9	33
KNN [11, 32]	98	6250	314	23	39	5	33
KNNTa	98	6250	493	19	51	5.1	42
KNNTa	98	5344	550	20	53	6.6	83
KNNTa-prec	98	7121	500	31	59	2.5	33
KNNTa-prec	97	6461	603	28	60	3.3	50

Table 3: Piezoelectric parameters for KNNTa-classic and KNNTa-prec samples.

4. Conclusion

In this study, Ta-substituted KNN ceramics were synthesized with two routes using different precursors and the SPS process, leading to high density materials. SEM-EDS analysis revealed the presence of several phases which were confirmed by XRD Rietveld refinement. Indeed, the alternative synthesis route with an pre-synthesized oxide precursor $Nb_{1.6}Ta_{0.4}O_5$ allows to better substitute the tantalum in the structure and to move to one main *Amm2* orthorhombic phase (92%) in addition with a small amount of a Ta-rich $Pm\bar{3}m$ cubic phase. Moreover, the Na/K ratio corresponding to main *Amm2* phase is similar to the one found at the MPB composition, frequently mentioned in the literature [34]. An enhancement of electromechanical coupling coefficients over 50% for k_t and over 15% for k_p, combined with lower electrical losses, is attributed to the successful substitution of Ta, the MPB composition control and the improvement of the composition homogeneity in the KNNTa-prec ceramics. This synthesis route combined to the efficiency of the Spark Plasma Sintering process can be used now for doping investigations such as Li or Mn to go further in the competition between PZT and the lead free materials. The reproductibility and the electromechanical properties obtained here might be now transfered to production processes and their applications.

5. Acknowledgement

We thank Mathieu Allix (CEMHTI CNRS UPR3079, Orléans, France) for conducting the TEM-EDS measurements, the ICMN laboratory (Orléans, France) for TEM access, Frédéric Dorvaux for his help in SPS experiments and Franck Levassort for his contribution in KLM fit. Use of the Advanced Photon Source at Argonne National Laboratory was supported by the U. S. Department of Energy, Office of Science, Office of Basic Energy Sciences, under Contract No. DE-AC02-06CH11357.

References

[1] M. D. Maeder, D. Damjanovic, N. Setter, **Lead-free piezoelectric materials**, J. Electroceram. 13 (1) (2004) pp. 385–392. doi:10.1007/s10832-004-5130-y.

[2] H. Wei, H. Wang, Y. Xia, D. Cui, Y. Shi, M. Dong, C. Liu, T. Ding, J. Zhang, Y. Ma, N. Wang, Z. Wang, Y. Sun, R. Wei, Z. Guo, **An overview of lead-free piezoelectric materials and devices**, J. Mater. Chem. C 6 (46) (2018) pp. 12446–12467. doi:10.1039/C8TC04515A.

[3] E. Aksel, J. L. Jones, **Advances in lead-free piezoelectric materials for sensors and actuators**, Sensors 10 (3) (2010) pp. 1935–1954. doi:10.3390/s100301935.

[4] P. K. Panda, **Review: environmental friendly lead-free piezoelectric materials**, J. Mater. Sci. 44 (19) (2009) pp. 5049–5062. doi:10.1007/s10853-009-3643-0.

[5] J. Acker, H. Kungl, M. J. Hoffmann, **Influence of alkaline and niobium excess on sintering and microstructure of sodium-potassium niobate ($K_{0.5}Na_{0.5}$)NbO_3**, J. Am. Ceram. Soc. 93 (5) (2010) pp. 1270–1281. doi:https://doi.org/10.1111/j.1551-2916.2010.03578.x.

[6] C.-W. Ahn, C.-S. Park, C.-H. Choi, S. Nahm, M.-J. Yoo, H.-G. Lee, S. Priya, **Sintering behavior of lead-free (K,Na)NbO_3 based piezoelectric ceramics**, J. Am. Ceram. Soc. 92 (9) (2009) pp. 2033–2038. doi:https://doi.org/10.1111/j.1551-2916.2009.03167.x.

[7] Y. Zhen, J.-F. Li, **Abnormal Grain growth and new core–shell structure in (K,Na)NbO_3-based lead-free piezoelectric ceramics**, J. Am. Ceram. Soc. 90 (11) (2007) pp. 3496–3502. doi:https://doi.org/10.1111/j.1551-2916.2007.01977.x.

[8] J. G. Fisher, S.-J. L. Kang, **Microstructural changes in ($K_{0.5}Na_{0.5}$)NbO_3 ceramics sintered in various atmospheres**, J. Eur. Ceram. Soc. 29 (12) (2009) pp. 2581–2588. doi:10.1016/j.jeurceramsoc.2009.02.006.

[9] B. Malic, J. Bernard, A. Bencan, M. Kosec, **Influence of zirconia addition on the microstructure of $K_{0.5}Na_{0.5}NbO_3$ ceramics**, J. Eur. Ceram. Soc. 28 (6) (2008) pp. 1191–1196. doi:10.1016/j.jeurceramsoc.2007.11.004.

[10] F. Jean, F. Schoenstein, M. Zaghrioui, M. Bah, P. Marchet, J. Bustillo, F. Giovannelli, I. Monot-Laffez, **Composite microstructures and piezoelectric properties**

in tantalum substituted lead-free $K_{0.5}Na_{0.5}Nb_{1-x}Ta_xO_3$ ceramics, Ceram. Int. 44 (8) (2018) pp.9463–9471. doi:10.1016/j.ceramint.2018.02.163.

[11] M. Bah, F. Giovannelli, F. Schoenstein, G. Feuillard, E. Le Clezio, I. Monot-Laffez, **High electromechanical performance with spark plasma sintering of undoped $K_{0.5}Na_{0.5}NbO_3$ ceramics**, Ceram. Int. 40 (5) (2014) pp. 7473–7480. doi:10.1016/j.ceramint.2013.12.097.

[12] J. A. Eiras, R. B. Z. Gerbasi, J. M. Rosso, D. M. Silva, L. F. Cótica, I. A. Santos, C. A. Souza, M. H. Lente, **Compositional design of dielectric, ferroelectric and piezoelectric properties of (K,Na)NbO_3 and (Ba,Na)(Ti,Nb)O_3 based ceramics prepared by different sintering routes**, Materials 9 (3) (2016) 179. doi:10.3390/ma9030179.

[13] J.-F. Li, K. Wang, B.-P. Zhang, L.-M. Zhang, **Ferroelectric and piezoelectric properties of fine–grained $Na_{0.5}K_{0.5}NbO_3$ lead-free piezoelectric ceramics prepared by Spark Plasma Sintering**, J. Am. Ceram. Soc. 89 (2) (2006) pp. 706–709. doi:10.1111/j.1551-2916.2005.00743.x.

[14] H. Zhang, X. Wang, J. Fang, Y. Zhang, L. Li, **Piezoelectric properties of Li, Sb, and Ta co-doped (K,Na)NbO_3 ceramics with fine grain size sintered by SPS method**, J. Electroceram. 30 (4) (2013) pp. 217–220. doi:10.1007/s10832-013-9787-y.

[15] Y. Wang, D. Damjanovic, N. Klein, E. Hollenstein, N. Setter, **Compositional inhomogeneity in Li- and Ta-modified (K,Na)NbO_3 ceramics**, J. Am. Ceram. Soc. 90 (11) (2007) pp. 3485–3489. doi:10.1111/j.1551-2916.2007.01962.x.

[16] E. Hollenstein, M. Davis, D. Damjanovic, N. Setter, **Piezoelectric properties of Li- and Ta-modified ($K_{0.5}Na_{0.5}$)NbO_3 ceramics**, Appl. Phys. Lett. 87 (18) (2005) 182905. doi:10.1063/1.2123387.

[17] R. López-Juárez, F. González-García, J. Zárate-Medina, R. Escalona-González, S. D. de la Torre, M.-E. Villafuerte-Castrejón, **Piezoelectric properties of Li–Ta co-**

doped potassium–sodium niobate ceramics prepared by spark plasma and conventional sintering, J. Alloys Compd. 509 (9) (2011) pp. 3837–3842. doi:10.1016/j.jallcom.2010.12.103.

[18] L. Wang, W. Ren, W. Ma, M. Liu, P. Shi, X. Wu, **Improved electrical properties for Mn-doped lead-free piezoelectric potassium sodium niobate ceramics**, AIP Adv. 5 (9) (2015) 097120. doi:10.1063/1.4930820.

[19] M. Asif Rafiq, A. Tkach, M. Elisabete Costa, P. Maria Vilarinho, **Defects and charge transport in Mn-doped $K_{0.5}Na_{0.5}NbO_3$ ceramics**, Phys. Chem. Chem. Phys. 17 (37) (2015) pp. 24403–24411. doi:10.1039/C5CP02883C.

[20] S. Zhang, R. Xia, T. R. Shrout, G. Zang, J. Wang, **Piezoelectric properties in perovskite 0.948 $(K_{0.5}Na_{0.5})NbO_3$ – 0.052 $LiSbO_3$ lead-free ceramics**, Journal of Applied Physics 100 (10) (2006) 104108. doi:10.1063/1.2382348.

[21] S. Zhang, R. Xia, T. R. Shrout, G. Zang, J. Wang, **Characterization of lead-free $(K_{0.5}Na_{0.5})NbO_3$ – $LiSbO_3$ piezoceramic**, Solid State Commun. 141 (12) (2007) pp. 675–679. doi:10.1016/j.ssc.2007.01.007.

[22] J. Bernard, A. Benčan, T. Rojac, J. Holc, B. Malič, M. Kosec, **Low-temperature sintering of $K_{0.5}Na_{0.5}NbO_3$ ceramics**, J. Am. Ceram. Soc. 91 (7) (2008) pp. 2409–2411. doi:https://doi.org/10.1111/j.1551-2916.2008.02447.x.

[23] M. Matsubara, K. Kikuta, S. Hirano, **Piezoelectric properties of $(K_{0.5}Na_{0.5})(Nb_{1-x}Ta_x)O_3$ – $K_{5.4}CuTa_{10}O_{29}$ ceramics**, J. Appl. Phys. 97 (11) (2005) 114105. doi:10.1063/1.1926396.

[24] L. Chen, G. Qiu, B. Peng, M. Guo, M. Zhang, **$(K_{0.5}Na_{0.5})(Nb_{1-x}Ta_x)O_3$ ceramics with a higher d_{33}: preparation from a two-stage microwave hydrothermal process**, Ceram. Int. 41 (10, Part A) (2015) pp. 13331–13340. doi:10.1016/j.ceramint.2015.07.117.

[25] Y. G. Lv, C. L. Wang, J. L. Zhang, L. Wu, M. L. Zhao, J. P. Xu, **Tantalum influence**

on physical properties of $(K_{0.5}Na_{0.5})(Nb_{1-x}Ta_x)O_3$ ceramics, Mater. Res. Bull. 44 (2) (2009) pp. 284–287. doi:10.1016/j.materresbull.2008.06.019.

[26] M. Matsubara, T. Yamaguchi, W. Sakamoto, K. Kikuta, T. Yogo, S.-i. Hirano, **Processing and piezoelectric properties of lead-free (K,Na)(Nb,Ta)O_3 ceramics**, J. Am. Ceram. Soc. 88 (5) (2005) pp. 1190–1196. doi:10.1111/j.1551-2916.2005.00229.x.

[27] A. Hussain, A. Maqbool, J. S. Kim, T. K. Song, M. H. Kim, W. J. Kim, S. S. Kim, **Sodium excess Ta-modified $(K_{0.5}Na_{0.5})NbO_3$ ceramics prepared by reactive template grain growth method**, Int. J. Appl. Ceram. Technol. 12 (1) (2015) pp. 228–234. doi:10.1111/ijac.12150.

[28] Y. Sung, J. Lee, S. Kim, T. Lee, J. Kim, J. Cho, T. Song, M. Kim, T. Park, **Enhanced piezoelectric properties of $(Na_{0.53}K_{0.47})(Nb_{1-x}Ta_x)O_3$ ceramics by Ta substitution**, Ceram. Int. 38 (2012) pp. S301–S304. doi:10.1016/j.ceramint.2011.04.106.

[29] F. Delorme, M. Bah, F. Schoenstein, F. Jean, M. Zouaoui Jabli, I. Monot-Laffez, F. Giovannelli, **Thermoelectric properties of oxygen deficient $(K_{0.5}Na_{0.5})NbO_3$ ceramics**, Mater. Lett. 162 (2016) pp. 24–27. doi:10.1016/j.matlet.2015.09.124.

[30] V. T. Tung, N. T. Tinh, N. H. Yen, D. A. Tuan, **Evaluation of electromechanical coupling factor for piezoelectric materials using finite element modeling**, Int. J. Mater. Sci. Chem. 3 (3) (2013) pp. 59–63. doi:10.5923/j.ijmc.20130303.03.

[31] M. Domenjoud, J. Bustillo, M. Lethiecq, L.-P. Tran-Huu-Hue, **Modelling of hysteretic behavior of piezoceramic materials under electrical loading**, Appl. Phys. Lett. 103 (17) (2013) 172903. doi:10.1063/1.4826180.

[32] M. Bah, F. Giovannelli, F. Schoenstein, G. Feuillard, E. L. Clezio, I. Monot-Laffez, **Synthesis, microstructure and electromechanical properties of undoped $(K_{0.5}Na_{0.5})NbO_3$**, Adv. Appl. Ceram. 114 (4) (2015) pp. 211–219. doi:10.1179/1743676114Y.0000000230.

[33] D. Kuscer, A. Kocjan, M. Majcen, A. Meden, K. Radan, J. Kovač, B. Malič, **Evolution of phase composition and microstructure of sodium potassium niobate –based ceramic during pressure-less spark plasma sintering and post-annealing**, Ceram. Int. 45 (8) (2019) pp. 10429–10437. doi:10.1016/j.ceramint.2019.02.102.

[34] Y. S. Sung, **Roles of Li and Ta in Pb-free piezoelectric (Na,K)NbO_3 ceramics**, Appl. Phys. Lett. 105 (14) (2014) 142903. doi:10.1063/1.4897642.

Site	**x**	**y**	**z**	**Occupancy**	**B_{iso} (Å^2)**
Na / K	0	0	0	0.507(4) / 0.493(4)	1.01(2)
Nb	0.5	0	0.5131(5)	1	0.282(4)
O1	0	0	0.4753(8)	1	0.63(5)
O2	0.5	0.7528(7)	0.2348(9)	1	0.94(3)
S.G.: *Amm2*; LPs: a = 3.94257(1), b = 5.64269(2), c = 5.67649(2) Å; V = 126.283(1) Å^3					

Table S1: Structural parameters for a sintered sample of $K_{0.5}Na_{0.5}NbO_3$ (KNN), refined against high resolution XRD data, corresponding to Fig. 5a of the main manuscript (R_{wp} = 10.47), χ^2 = 1.549).

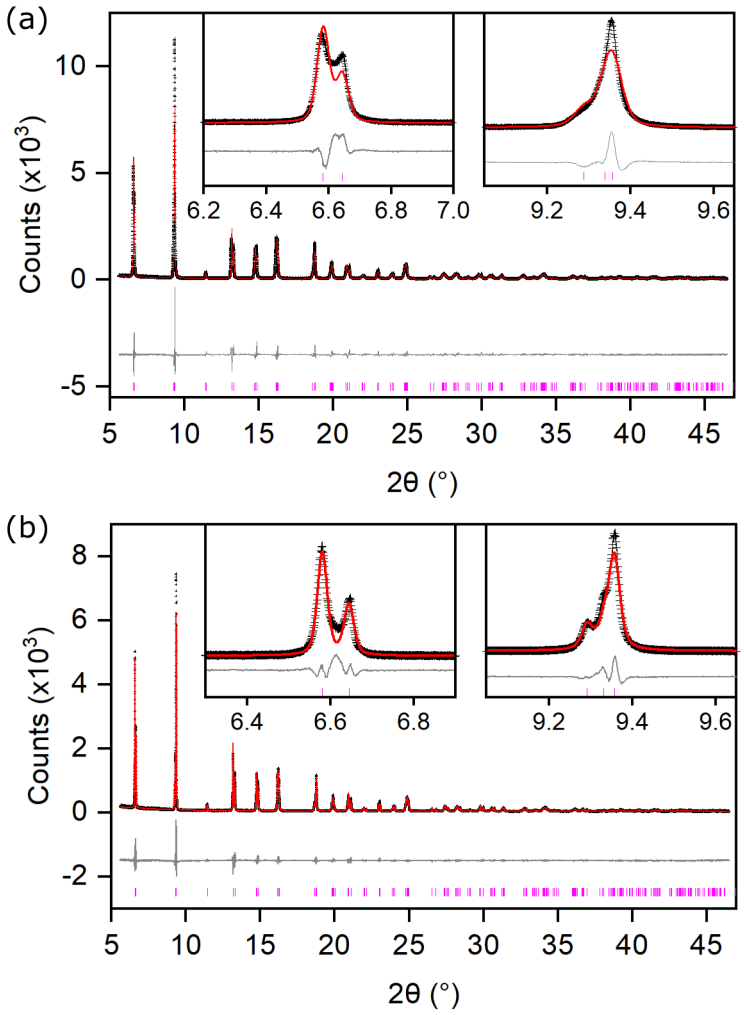

Figure S1: Single-phase Rietveld refinements for (a) KNNTa and (b) KNNTa-prec, using only the Amm2 phase with the nominal composition $K_{0.5}Na_{0.5}Nb_{0.8}Ta_{0.2}O_3$. Magnified views of the (011)/(100) peaks and the (002)/(020)/(111) peaks are shown as insets. This produced agreement factors $R_{wp} = 14.17$, $\chi^2 = 3.56$ for KNNTa, and $R_{wp} = 12.24$, $\chi^2 = 1.62$ for KNNTa-prec.

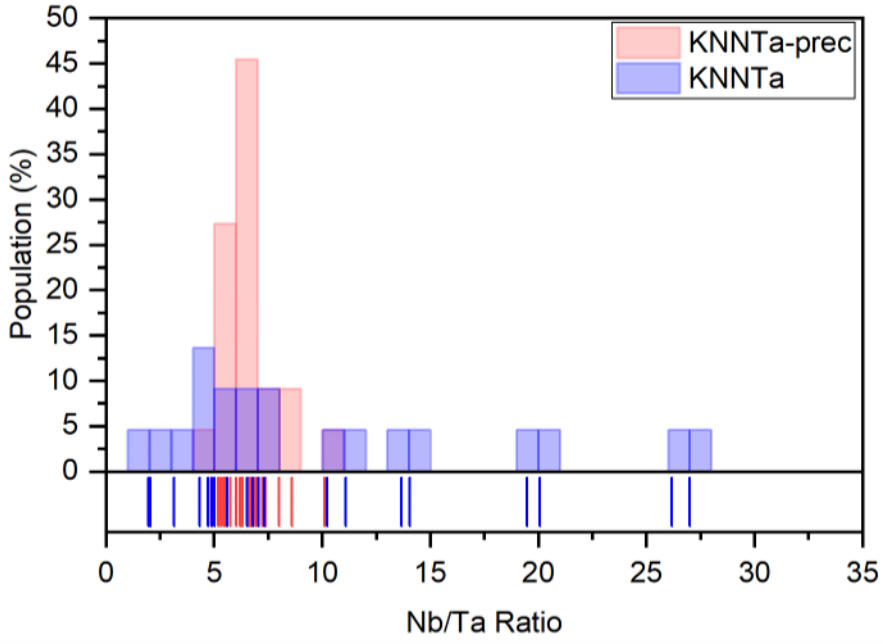

Figure S2: TEM-EDS results from 20 particles of KNNTa (blue markers/bars) and KNNTa-prec (red markers/bars), with compositions plotted as Nb/Ta ratio. The KNNTa-prec compositions are tightly clustered, whilst the KNNTa compositions are spread over a wide range. Note that Na and K were not analysed due to their volatility in the electron beam.